SUPPORTING INFORMATION FOR

Diversification, disparification, and hybridization in the desert shrubs *Encelia*

Sonal Singhal, Adam B. Roddy, Christopher DiVittorio, Ary Sanchez-Amaya, Claudia L. Henriquez, Craig R. Brodersen, Shannon Fehlberg, Felipe Zapata

Supplementary Methods

Sampling: Common Garden

Collected seeds were planted in a common garden for use in all genetic and phenotypic analyses. The common garden was first planted in 2011 and then expanded in 2016. By using a common garden to collect both genetic and phenotypic data, we ensured that our phenotypic data were matched to a genotype and that phenotypic differences among individuals were not due to environmental variation. Seeds were germinated in greenhouse trays using an equal mix of pumice, sand, and vermiculite. *Encelia ravenii* and *E. resinifera* were not included in the garden because their seeds failed to germinate. When seedlings were 5 cm tall or had four true leaves, they were transplanted into the common garden at the University of California Agricultural Operations Station in Riverside, CA. Seedlings were randomized across rows and then irrigated weekly. Plants were phenotyped from 2015 to 2016, and in October 2016, adult leaves were collected in silica gel for use in genetic analysis. For phenotypic measurements of *E. ravenii* and *E. resinifera*, we used field-collected adult leaves.

Genetic data collection

Because ddRAD data have not yet been collected for *Encelia*, we first conducted a series of *in silico* experiments to determine the best restriction enzymes and target size to use. The closest available reference genome to *Encelia* is *Helianthus annuus*, another species of the family Asteraceae estimated to be 7.5 million years diverged from *Encelia* (Smith & Brown, 2018). Many of the species in Asteraceae, including *Encelia*, have extensive repetitive content (Badouin *et al.*, 2017). To avoid sequencing this repeat content, we focused on testing restriction enzymes that are sensitive to the DNA methylation common in repeat content (Pegadaraju *et al.*, 2013). In total, we tested 14 different restriction enzymes in all possible

pairwise combinations. Ultimately, to give the desired yield of 20,000 loci, we used *PstI* and *MspI*, size-selecting between 250 - 700 bp.

To collect ddRAD data, we first extracted DNA from silica-dried adult leaves using a QIAGEN DNeasy Plant Kit (cat. no.: 69104) following manufacturer's instructions. We determined DNA quality by running extracts on a 2% agarose gel and DNA concentration by using a NanoDrop DNA spectrometer. The commercial provider RTL Genomics (Lubbock, TX, USA) then prepared doubly-barcoded ddRAD libraries (Peterson *et al.*, 2012). Equimolar amounts of samples were combined to generate pools of 100 individuals; each pool was sequenced across one lane of 100 PE sequencing on the Illumina HiSeq 4000 Sequencing Platform.

Per individual, we first cleaned all reads, trimming adaptors and low quality sequence using `Trimmomatic v36` (Bolger *et al.*, 2014). We then merged any overlapping reads using `PEAR v0.9.8` (Zhang *et al.*, 2014). Due to extensive adaptor contamination, many of our paired reads became orphaned through the cleaning process. We then assembled cleaned and merged reads using `Velvet v1.2.10` (Zerbino & Birney, 2008) across multiple k-mer values. Although `Velvet` is not often used in ddRAD assembly, other commonly used tools like `Rainbow` or `STACKS` are not designed to assemble mixed sets of single-end and paired-end reads. We then retained all assembled loci with coverage ≥2×, resulting in an average of 140K loci per individual.

Phylogenetic Inference

Although all sampled individuals were identified to nominal species, species boundaries have not been well-tested in *Encelia*. Thus, our first set of analyses were designed to determine lineage identity per individual. We used `VSEARCH v2.9.1` (Rognes *et al.*, 2016) to identify homologous loci using a 70% identity cutoff. After aligning homologous loci using `mafft v7.9.34` (Katoh *et al.*, 2009), we then concatenated homologous loci across individuals, removing any individual sequenced for <5% of loci or any loci sequenced for <30% of individuals. We used `RAxML v8.2.11` to generate a phylogeny from the 11.6K locus, 1.5 Mb concatenated alignment (Stamatakis, 2014). By comparing clade identity to nominal species identity, we determined likely lineage identities for each individual (Table S1).

We then inferred individual-level phylogenies using both concatenated and coalescent-based approaches. First, we used the lineage-level pseudo-reference genomes and the variant call set to determine loci sequences per individual. We removed any sequences with >30% of missing sites and any loci sampled for <60% of individuals. We then used RAxML to infer a phylogeny and 100 bootstraps from the 31K locus, 3.9 Mb concatenated alignment. For a coalescent-based approach, we used SVDquartets (Chifman & Kubatko, 2014). We randomly sampled one SNP per locus, retaining SNPs with <20% missing and ≥2 minor allele count. We used the resulting set of 2.8K SNPs to infer the phylogeny and to conduct 100 bootstrap analyses. Bootstrap estimates of nodal support are often inflated, particularly for phylogenomic datasets (Cummings *et al.*, 2003). Accordingly, we calculated gene concordance factors (gCF) and site concordance factors (sCF) using IQ-TREE v1.6.4 (Minh *et al.*, 2020), both of which better measure conflict across loci and sites.

Then, we used two different coalescent-based approaches - one based on gene trees and the other based on SNPs - to infer a lineage-level phylogeny. We used ASTRAL-III (Zhang *et al.*, 2018), which, when given an individual-to-lineage mapping and a set of gene trees inferred across individuals, can generate a lineage-level phylogeny. Here, we filtered loci to include only loci inferred for >60% of individuals, inferred gene trees using RAxML, collapsed all randomly-bifurcated nodes using 'dimulti' in the R package ape (Paradis *et al.*, 2004), and then inferred the species tree from these gene trees with ASTRAL-III. Second, using the same SNP dataset used for the individual-level SVDquartets analysis, we additionally inferred a lineage-level phylogeny. Neither ASTRAL-III nor SVDquartets provides terminal branch lengths. Accordingly, to infer an ultrametric phylogeny for use in comparative analyses, we generated a lineage-level concatenated alignment by randomly selecting one sequence per locus per lineage. We then used RAxML to estimate branch lengths, constraining the topology to each of the lineage-level phylogenies. To infer an ultrametric tree for this group, we used a calibration from a comprehensive angiosperm phylogeny that estimated the crown age of *Encelia* as 1.36 million years (Myr) (Magallón *et al.*, 2015; Smith & Brown, 2018). This aligns with previous divergence dating based on population genomic data that inferred the root of *Encelia* as 1.05 Myr (Singhal, unpublished). We used this root age to infer an ultrametric tree using the 'chronos' function in the R package 'ape' with lambda of 0.01.

MicroCT imaging

High-resolution, three-dimensional (3D) images of stem and leaf structure were obtained by performing hard X-ray microcomputed tomography (microCT) at the Advanced Light Source, Lawrence Berkeley National Laboratory (LBNL), Beamline 8.3.2 (Brodersen, 2013; Brodersen & Roddy, 2016). These images were used to visualize fine-scale morphology and anatomy of these leaves and to calculate trichome density and stem xylem vessel diameter and area. Leaf samples were collected from plants growing in cultivation at the Agricultural Operations Station, University of California, Riverside in June 2015 and September 2016 and transported to LBNL, keeping the leaves hydrated until imaging. Samples were placed on a rotating stage in the 24 keV synchrotron X-ray beam and continuously rotated from 0 to 180 degrees. As the sample rotated continuously through the beam, 1025 two-dimensional projections were recorded using a 10x objective, yielding a final pixel resolution of 1.25 µm. Each scan was completed in ~15 min. These raw tomographic projections were reconstructed using TomoPy, a Python-based framework for reconstructing tomographic data (Gürsoy *et al.*, 2014). Images were reconstructed using gridrec (Dowd *et al.*, 1999) and phase retrieval (Davis *et al.*, 1995) reconstruction methods. Image stacks were rotated, aligned, and traits measured in FIJI (Schindelin *et al.*, 2012). Three-dimensional stack visualization was performed in Avizo v. 9.2.0 (ThermoFisher Scientific).

Trait data collection & analysis

Leaf area, shape, and color

To analyze leaf area, shape, and color, we collected three to five adult leaves per individual growing in the common garden. Using a digital camera, we photographed these leaves with a black-and-white reference scale bar. Leaves were then oven-dried at 70 C for at least 72 hours and weighed for dry mass using a Sartorius Practum (resolution of 0.0001 mg, Sartorius AG, Goettingen, Germany). We analyzed leaf images using ImageJ (Rasband & Others, 1997), first calibrating the white balance and size of each image using the scale bar as a reference (Mascalchi, 2017). For each leaf, we set the threshold across the leaf, excluding the petiole, and then collected data on area, perimeter, fit ellipse, and shape using the Analyze Particles function. To measure color, we used the white-balanced leaf images in Adobe Photoshop and

measured the arithmetic mean of all pixels of the largest circumscribed rectangle possible within the center of the leaf. We calculated leaf mass per area (LMA) using measurements of leaf area and dry mass. We conducted a principal component analysis of all leaf size and shape measurements after centering and scaling them. The first two axes summarize 42% and 24% of the variation respectively; PC1 largely loads on size-related measurements and PC2 largely reflects the roundness of the leaf.

Canopy ramification

We estimated the degree of canopy ramification as the number of terminal branch tips per stem cross-sectional area (BTSA; Roddy *et al.*, 2019). For each plant in the common garden, we took two perpendicular measurements of the diameter of the stem base using manual calipers and averaged these two measurements to estimate the area of the stem base. We then counted all branch tips descendant from this base, regardless of their size.

Trichome density

Trichomes were characterized from 3D microCT images of fresh leaves. Subregions of each leaf surface were cropped and rotated to align the leaf surface with the plane of view. Digital slices parallel to the leaf surface were taken through the trichomes, allowing trichomes to be counted per unit projected leaf surface area.

Vessel dimensions

Stem xylem vessel dimensions were measured from 2D cross sections of microCT image stacks obtained from dried stems. Images were thresholded and binarized to distinguish vessel lumens from plant tissue, and the area of each of these lumens measured using the Analyze Particles function in ImageJ.

Wood density

Wood density was measured using Archimedes' principle. A small segment of stem was excised, its bark removed, and its volume measured as the mass of water displaced when it was submerged in a beaker of water sitting on a balance. The segment was then oven-dried at 70 C for at least one week, after which its dry mass was measured.

Stem hydraulic conductance

Whole-shoot hydraulic conductance was measured using a low pressure flow meter (Kolb *et al.*, 1996), which enables measuring the entire shoot regardless of branch ramification and can be applied to morphologically diverse structures (Roddy *et al.*, 2016, 2019). Mature plants growing under well-watered conditions at the Agricultural Operations Station, University of California, Riverside, were sampled in May 2013. Healthy shoots were selected from each plant.

In the late evening, entire shoots were cut at their base, and immediately recut underwater while the shoot was enclosed in black plastic bags and transported to the lab. Shoots were allowed to rehydrate for at least two hours before hydraulic measurements, and measurements were completed within 24 hours of sampling. Branching shoots were defoliated underwater, the leaves scanned for leaf area, and the cut shoot base was recut under clean water with a fresh razor blade. While keeping the cut stem surface covered in water, the shoot base was quickly enclosed in a compression fitting that was connected to a hard-sided tube, which was filled with and plumbed back to a bottle of 0.01 M KCl that sat on a microbalance with resolution to 0.0001 g (Sartorius CPA225D, Sartorius AG, Goettingen, Germany). The shoot was enclosed in an acrylic vacuum chamber. The vacuum chamber was connected to a pressure gauge and a vacuum pump, which created a series of partial vacuums (60, 50, 40, 30, 20, 15 kPa below ambient) on the stem that pulled KCl from the balance and into the stem. Every fifteen seconds the mass of KCl on the balance was logged by a computer interfaced with the balance (WinWedge, TAL Technologies Inc., Philadelphia, PA, USA). The partial vacuum was maintained for at least three minutes at each pressure and until the coefficient of variation of the previous ten measurements was below 0.05. The average of these last ten measurements was taken as the flow rate at the given pressure. Hydraulic conductance was calculated as the slope of the regression of flow rate versus pressure, and no more than one of the six measurements for each shoot was removed to improve linearity. Because shoots differed in size and ramification, hydraulic conductance was normalized by leaf area of the shoot, which is taken as a metric of hydraulic efficiency (Roddy *et al.*, 2019).

References

Badouin H, Gouzy J, Grassa CJ, Murat F, Staton SE, Cottret L, Lelandais-Brière C, Owens GL, Carrère S, Mayjonade B, *et al.* 2017. The sunflower genome provides insights into oil metabolism, flowering and Asterid evolution. *Nature* **546**: 148–152.

Bolger AM, Lohse M, Usadel B. **2014**. Trimmomatic: a flexible trimmer for Illumina sequence data. *Bioinformatics* **30**: 2114–2120.

Brodersen CR. **2013**. Visualizing wood anatomy in three dimensions with high-resolution X-ray micro-tomography (µCT) – a review. *IAWA Journal* **34**: 408–424.

Brodersen CR, Roddy AB. **2016**. New frontiers in the three-dimensional visualization of plant structure and function. *American journal of botany* **103**: 184–188.

Chifman J, Kubatko L. **2014**. Quartet inference from SNP data under the coalescent model. *Bioinformatics* **30**: 3317–3324.

Cummings MP, Handley SA, Myers DS, Reed DL, Rokas A, Winka K. **2003**. Comparing bootstrap and posterior probability values in the four-taxon case. *Systematic biology* **52**: 477–487.

Davis TJ, Gao D, Gureyev TE, Stevenson AW, Wilkins SW. **1995**. Phase-contrast imaging of weakly absorbing materials using hard X-rays. *Nature* **373**: 595–598.

Dowd BA, Campbell GH, Marr RB, Nagarkar VV, Tipnis SV, Axe L, Peter Siddons D. **1999**. Developments in synchrotron x-ray computed microtomography at the National Synchrotron Light Source. In: Developments in X-Ray Tomography II. International Society for Optics and Photonics, 224–236.

Gürsoy D, De Carlo F, Xiao X, Jacobsen C. **2014**. TomoPy: a framework for the analysis of synchrotron tomographic data. *Journal of synchrotron radiation* **21**: 1188–1193.

Katoh K, Asimenos G, Toh H. **2009**. Multiple alignment of DNA sequences with MAFFT. *Methods in Molecular Biology* **537**: 39–64.

Kolb KJ, Sperry JS, Lamont BB. **1996**. A method for measuring xylem hydraulic conductance and embolism in entire root and shoot systems. *Journal of Experimental Botany* **47**: 1805–1810.

Magallón S, Gómez‑Acevedo S, Sánchez‑Reyes LL, Hernández‑Hernández T. **2015**. A metacalibrated time-tree documents the early rise of flowering plant phylogenetic diversity. *The New Phytologist* **207**: 437–453.

Mascalchi P. **2017**. ImageJ Auto White Balance Correction. *ImageJ Auto White Balance Correction*.

Minh BQ, Hahn MW, Lanfear R. **2020**. New methods to calculate concordance factors for phylogenomic datasets. *Molecular Biology and Evolution* **in press**.

Paradis E, Claude J, Strimmer K. **2004**. APE: Analyses of Phylogenetics and Evolution in R language. *Bioinformatics* **20**: 289–290.

Pegadaraju V, Nipper R, Hulke B, Qi L, Schultz Q. **2013**. De novo sequencing of sunflower genome for SNP discovery using RAD (Restriction site Associated DNA) approach. *BMC genomics* **14**: 556.

Peterson BK, Weber JN, Kay EH, Fisher HS, Hoekstra HE. **2012**. Double digest RADseq: an inexpensive method for de novo SNP discovery and genotyping in model and non-model species. *PloS one* **7**: e37135.

Rasband WS, Others. **1997**. ImageJ.

Roddy AB, van Blerk JJ, Midgley JJ, West AG. **2019**. Ramification has little impact on shoot hydraulic efficiency in the sexually dimorphic genus *Leucadendron* (Proteaceae). *PeerJ* **7**: e6835.

Roddy AB, Brodersen CR, Dawson TE. **2016**. Hydraulic conductance and the maintenance of water balance in flowers. *Plant, Cell & Environment* **39**: 2123–2132.

Rognes T, Flouri T, Nichols B, Quince C, Mahé F. **2016**. VSEARCH: a versatile open source tool for metagenomics. *PeerJ* **4**: e2584.

Schindelin J, Arganda-Carreras I, Frise E, Kaynig V, Longair M, Pietzsch T, Preibisch S,

Rueden C, Saalfeld S, Schmid B, *et al.* 2012. Fiji: an open-source platform for biological-image analysis. *Nature methods* **9**: 676–682.

Smith SA, Brown JW. **2018**. Constructing a broadly inclusive seed plant phylogeny. *American Journal of Botany* **105**: 302–314.

Stamatakis A. **2014**. RAxML version 8: a tool for phylogenetic analysis and post-analysis of large phylogenies. *Bioinformatics* **30**: 1312–1313.

Zerbino DR, Birney E. **2008**. Velvet: algorithms for *de novo* short read assembly using *de Bruijn* graphs. *Genome Research* **18**: 821–829.

Zhang J, Kobert K, Flouri T, Stamatakis A. **2014**. PEAR: a fast and accurate Illumina Paired-End reAd mergeR. *Bioinformatics* **30**: 614–620.

Zhang C, Rabiee M, Sayyari E, Mirarab S. **2018**. ASTRAL-III: polynomial time species tree reconstruction from partially resolved gene trees. *BMC bioinformatics* **19**: 153.

Supplementary Tables

Table S1: Information on the 72 individuals included in this study, including their species identification, the locality from which they were collected, and whether they are in our common garden. For those nominal species that contain multiple putative lineages, we indicate lineage identity in parentheses. This table also outlines the efficacy of our genetic data collection, including trimmed sequencing read yield in megabases (Mb), number of assembled homologous loci, and number of high-quality, high coverage variant and invariant sites.

sample	species	locality	In common garden	read yield (Mb)	loci count	sites (Mb)	SRA
ACT-9M-1	*Encelia actoni*	9 Mile Canyon Road, CA, USA	*	2055.59	68861	12.62	TBD
ACT-9M-2	*E. actoni*	9 Mile Canyon Road, CA, USA	*	223.83	37805	5.29	TBD
ACT-AB-1	*E. actoni*	Anza Borrego, CA, USA	*	176.34	33263	4.78	TBD
ACT-AB-2	*E. actoni*	Anza Borrego, CA, USA	*	102.6	22625	3.17	TBD
ASP-CD-1	*E. asperifolia*	Central Desert, BC, Mexico	*	72.55	19214	2.27	TBD
ASP-CD-2	*E. asperifolia*	Central Desert, BC, Mexico	*	308.75	37977	5.46	TBD
ASP0129	*E. asperifolia*	10 km south of El Rosarito, BC, Mexico		87.05	20879	2.45	TBD
CAL-CR-1	*E. californica (1)*	north of El Rosario, BC, Mexico	*	79.68	17522	2.21	TBD
CAL-CR-2	*E. californica (1)*	north of El Rosario, BC, Mexico	*	64.54	13257	1.72	TBD
CAL-SC-1	*E. californica (1)*	San Clemente, CA, USA	*	177.14	23995	3.38	TBD
CAL-SC-2	*E. californica (1)*	San Clemente, CA, USA	*	214.8	27656	4.25	TBD
CAL-ELR-1	*E. californica (2)*	pass south of El Rosario, BC, Mexico	*	72.35	13977	1.86	TBD
CAL-ELR-2	*E. californica (2)*	pass south of El Rosario, BC, Mexico	*	78.58	17616	2.24	TBD
CAN-COP-5	*E. canescens*	Atacama Desert, Chile		384.14	40606	6.47	TBD
CAN-DOM-1	*E. canescens*	Atacama Desert, Chile		483.94	13355	1.07	TBD
CAN-HUA-4	*E. canescens*	Atacama Desert, Chile		494.51	42540	7.26	TBD
CAN-HUA-6	*E. canescens*	Atacama Desert, Chile		325.6	27905	4.76	TBD

CAN-ING-1	*E. canescens*	Atacama Desert, Chile		122.41	14309	2.31	TBD
CAN-OBI-7	*E. canescens*	Atacama Desert, Chile		330.76	32032	5.26	TBD
CAN-OBI-9	*E. canescens*	Atacama Desert, Chile		85.97	18302	2.26	TBD
CAN-PERU-2	*E. canescens*	Arequipa 2, Peru	*	4091.65	49865	11.81	TBD
CAN-PERU-3	*E. canescens*	Mollebaya, Peru	*	1162.26	67133	8.96	TBD
CAN-VAL-9	*E. canescens*	Atacama Desert, Chile		769.06	62575	8.03	TBD
DEN-12-A	*E. densifolia*	Sierra Santa Clara, BCS, Mexico	*	513.66	55393	6.67	TBD
DEN-13-A	*E. densifolia*	Sierra Santa Clara, BCS, Mexico	*	323.22	52031	6.17	TBD
DEN-16	*E. densifolia*	Sierra Santa Clara, BCS, Mexico	*	966.03	77650	10.23	TBD
DEN-17	*E. densifolia*	Sierra Santa Clara, BCS, Mexico	*	279.31	50346	6.03	TBD
DEN-18-A	*E. densifolia*	Sierra Santa Clara, BCS, Mexico	*	365.55	52963	6.49	TBD
DEN-21	*E. densifolia*	Sierra Santa Clara, BCS, Mexico	*	42.47	16433	1.44	TBD
FAR-FAR-AB-1	*E. farinosa farinosa*	Anza Borrego, CA, USA	*	1186.43	90436	12.04	TBD
FAR-FAR-AB-2	*E. farinosa farinosa*	Anza Borrego, CA, USA	*	1905.66	96822	13.27	TBD
FAR-FAR-DVHZ-1	*E. farinosa farinosa*	Death Valley, CA, USA	*	815.27	79334	10.01	TBD
FAR-FAR-DVHZ-2	*E. farinosa farinosa*	Death Valley, CA, USA	*	1381.38	87741	11.83	TBD
FAR-FAR-DVSC-1	*E. farinosa farinosa*	Surprise Canyon, Death Valley, CA, USA	*	514.03	70868	8.93	TBD
FAR-FAR-HH-1	*E. farinosa farinosa*	Hidden Hills, Mojave National Preserve, CA, USA	*	419.46	60795	7.14	TBD
FAR-FAR-HH-2	*E. farinosa farinosa*	Hidden Hills, Mojave National Preserve, CA, USA	*	1324.88	88721	11.87	TBD
FAR-FAR-RV-1	*E. farinosa farinosa*	Riverside, CA, USA	*	356.7	65021	7.91	TBD
FAR-FAR-RV-2	*E. farinosa farinosa*	Riverside, CA, USA	*	1258.34	87994	11.57	TBD
FAR-PHE-52	*E. farinosa phenicodonta*	Central Desert, BC, Mexico	*	675.51	77547	9.94	TBD
FAR-PHE-60-2	*E. farinosa phenicodonta*	Sea of Cortez, BC, Mexico	*	892.79	77349	9.88	TBD
FAR-PHE-71-1	*E. farinosa phenicodonta*	north of San Felipe, BC, Mexico	*	865.67	84450	11.11	TBD
FAR-PHE-73-1	*E. farinosa phenicodonta*	north of San Felipe, BC, Mexico	*	696.14	71950	9.2	TBD

FAR-SON	*E. farinosa phenicodonta*	Sonora, Mexico	*	548.82	70368	8.6	TBD
FRU-FRU-DV-1	*E. frutescens frutescens*	Death Valley, CA, USA	*	416.43	61365	7.45	TBD
FRU-FRU-DV-2	*E. frutescens frutescens*	Death Valley, CA, USA	*	456.33	59658	7.13	TBD
FRU-FRU-DVHZ-1	*E. frutescens frutescens*	Death Valley, CA, USA	*	1019.08	76237	9.68	TBD
FRU-FRU-DVHZ-2	*E. frutescens frutescens*	Death Valley, CA, USA	*	683.58	70228	8.81	TBD
FRU-FRU-MNP-1	*E. frutescens frutescens*	Mojave National Preserve, CA, USA	*	814.49	77813	9.78	TBD
FRU-FRU-MNP-2	*E. frutescens frutescens*	Mojave National Preserve, CA, USA	*	1115.06	85680	11.03	TBD
FRUGLA1	*E. frutescens glandulosa*	25 km north of Condensadora, BC, Mexico		1570.74	94144	12.62	TBD
FRUGLA2	*E. frutescens glandulosa*	25 km north of Condensadora, BC, Mexico		462.31	69256	8.24	TBD
PAL-BA-1	*E. palmeri*	Bahia Asuncion, BCS, Mexico	*	59.69	20398	1.81	TBD
PAL-BA-2	*E. palmeri*	Bahia Asuncion, BCS, Mexico	*	1305.15	90331	12.08	TBD
PAL-JESUS-01	*E. palmeri*	Villa Jesus Maria, BC, Mexico		903.89	79699	10.43	TBD
PAL648	*E. palmeri*	El Marasal, BC, Mexico		1143.91	87751	11.71	TBD
RAV-1	*E. ravenii*	San Felipe Desert, BC, Mexico		1763.21	85833	11.45	TBD
RAV-10	*E. ravenii*	San Felipe Desert, BC, Mexico		1971.25	92493	12.62	TBD
RAV-11	*E. ravenii*	San Felipe Desert, BC, Mexico		1224.63	72385	9.89	TBD
RAV-13	*E. ravenii*	San Felipe Desert, BC, Mexico		1577.5	87206	11.73	TBD
RAV-2	*E. ravenii*	San Felipe Desert, BC, Mexico		1231.7	84033	11.05	TBD
RES-1	*E. resinifera*	Zion National Park, Washington Co., UT, USA		919.69	91989	12.08	TBD
RES-2	*E. resinifera*	Zion National Park, Washington Co., UT, USA		1322.5	98559	13.05	TBD
VEN-BA-1	*E. ventorum*	Bahia Asuncion, BCS, Mexico	*	1452.92	89500	11.71	TBD
VEN-BA-2	*E. ventorum*	Bahia Asuncion, BCS, Mexico	*	2350.32	97483	13.31	TBD

VIR-GMDRC	*E. virginensis (1)*	Granite Mountains Desert Research Center, CA, USA	*	1575.73	96090	12.92	TBD
VIR-MNP-1	*E. virginensis (1)*	Foshay Pass, Mojave National Preserve, CA, USA	*	871.66	84453	11.29	TBD
VIR-MNP-2	*E. virginensis (1)*	Foshay Pass, Mojave National Preserve, CA, USA	*	1792.58	98577	13.66	TBD
VIR-UT-1	*E. virginensis (2)*	Highway 91, Washington Co., UT, USA		1565.36	108361	14.61	TBD
VIR-UT-2	*E. virginensis (2)*	Highway 91, Washington Co., UT, USA		637.33	71703	9.24	TBD
ENC-1	*Enceliopsis covillei*	Surprise Canyon, Death Valley, CA, USA	*	1066.09	48713	5.99	TBD
ENC-2	*Enceliopsis covillei*	Surprise Canyon, Death Valley, CA, USA	*	1378.21	49010	6.34	TBD
XYL	*Xylorhiza tortifolia*	Mojave National Preserve, CA, USA	*	2756.57	10268	0.93	TBD

Table S2: The nine morphological and physiological traits measured in this study.

trait	description	# of lineages measured
canopy ramification	measured as the number of branch tips per stem cross-sectional area (BTSA)	15
trichome density	top and bottom trichome density was measured on microCT leaf images; top and bottom trichome density were highly correlated (r = 0.99, p-val < 5e-14)	15
stem hydraulic conductance	slope of flow rate versus pressure for stems, normalized by leaf area of shoot	8
leaf color	leaf color was calculated on color-balanced leaves as the arithmetic mean of pixels	12
leaf roundness	leaf roundness is highly correlated with leaf PC2 (r = -0.98) which captures 24% of the variation	12
leaf area	leaf area is highly correlated with leaf PC1 (r = -0.97, p-val < 2e-16) which captures 42.5% of the variation	12
leaf mass area (LMA)	leaf dry mass divided by leaf area	12
wood density	woody stem (stripped of bark) dry mass divided by its volume	5
vessel diameter	stem xylem vessel diameter	11

Table S3: Results of significant D-statistic tests. Shown are D-statistic analyses that significantly deviate from 0, as measured by their Z-score. The two species inferred to have exchanged genes, as determined by the sign of the D-statistic, are listed in the first two columns.

species 1	species 2	D-statistic	Z-score	p-val
E. actoni	*E. virginensis 1*	0.19	34.66	3.12E-263
E. actoni	*E. frutescens frutescens*	0.06	8.52	1.62E-17
E. virginensis 1	*E. frutescens frutescens*	0.04	6.5	7.96E-11
E. californica 1	*E. californica 2*	0.1	5.13	2.86E-07
E. palmeri	*E. farinosa farinosa*	0.11	7.07	1.55E-12
E. palmeri	*E. farinosa phenicodonta*	0.03	6.17	6.79E-10
E. palmeri	*E. ravenii*	0.03	4.62	3.83E-06
E. ravenii	*E. frutescens frutescens*	0.03	5.44	5.40E-08
E. frutescens frutescens	*E. virginensis 2*	0.04	6.97	3.06E-12
E. frutescens glandulosa	*E. virginensis 2*	0.07	10.73	7.73E-27

Table S4: Instances of hybridization and introgression in the *Encelia* genus. Shown are the involved species, what type of data was used to infer the hybridization or introgression event, and notes, including the reference for the data. Data types "dstat" and "SNaQ" come from the present study.

species 1	species 2	data type	notes
E. actoni	*E. frutescens*	natural hybrids	no explicit data, Clark 1998
E. actoni	*E. frutescens frutescens*	dstat	conservative test
E. actoni	*E. frutescens frutescens*	hybrid species	result in *E. virginensis*; genetic analysis from Allan et al 1997
E. actoni	*E. frutescens glandulosa*	hybrid species	result in *E. resinifera*; no formal test but included in Allan et al. 1997
E. actoni	*E. virginensis* 1	dstat	conservative test
E. asperifolia	*E. californica*	natural hybrids	field data from DiVittorio et al., unpublished
E. asperifolia	*E. californica* 2	SNaQ	approximately 50% admixture
E. asperifolia	*E. canescens*	dstat	conservative test
E. asperifolia	*E. farinosa*	natural hybrids	no explicit data, Clark 1998
E. asperifolia	*E. palmeri*	natural hybrids	field data from DiVittorio et al., unpublished
E. asperifolia	*E. ventorum*	natural hybrids	Kyhos et al. 1981; DiVittorio et al. 2020; Clark 1998
E. californica	*E. farinosa*	natural hybrids	http://nathistoc.bio.uci.edu/plants/Asteraceae/Encelia%20hybrids/Encelia%20hybrids.htm
E. californica	*E. frutescens*	hybrid species	result in *E. asperifolia*; no formal test but included in Allan et al. 1997
E. californica 1	*E. californica* 2	dstat	conservative test
E. californica 2	*E. farinosa*	dstat	conservative test

	phenicodonta		
E. densifolia	*E. farinosa*	natural hybrids	field data from DiVittorio et al., unpublished
E. farinosa	*E. frutescens*	natural hybrids	field data from DiVittorio et al., unpublished; Clark 1998
E. farinosa	*E. palmeri*	hybrid species	result in *E. canescens*; no formal test but included in Allan et al. 1997
E. farinosa	*E. palmeri*	natural hybrids	no explicit data, Clark 1998
E. farinosa farinosa	*E. palmeri*	dstat	conservative test
E. farinosa phenicodonta	*E. palmeri*	dstat	conservative test
E. frutescens	*E. virginensis*	natural hybrids	no explicit data, Clark 1998
E. frutescens frutescens	*E. ravenii*	dstat	conservative test
E. frutescens frutescens	*E. virginensis* 1	dstat	conservative test
E. frutescens frutescens	*E. virginensis* 2	dstat	conservative test
E. frutescens glandulosa	*E. virginensis* 2	dstat	conservative test
E. palmeri	*E. ravenii*	dstat	conservative test
E. palmeri	*E. ventorum*	natural hybrids	Kyhos et al. 1981; DiVittorio et al. 2020; Clark 1998
E. palmeri	*E. virginensis* 2	dstat	conservative test

Table S5: Expected correlations between traits and different environmental variables and the correlation recovered in this study, and whether or not it is significant (sig.) or not (n.s.). Abbreviations follow Table 1.

trait	environmental variable	predicted correlation	found correlation
trichomes	precipitation	-	+, n.s.
trichomes	temperature	+	+, n.s.
leaf area	precipitation	+	+, n.s.
leaf area	temperature	-	-, n.s.
LMA	precipitation	+	+, n.s.
LMA	temperature	+	+, sig.

Supplementary Figures
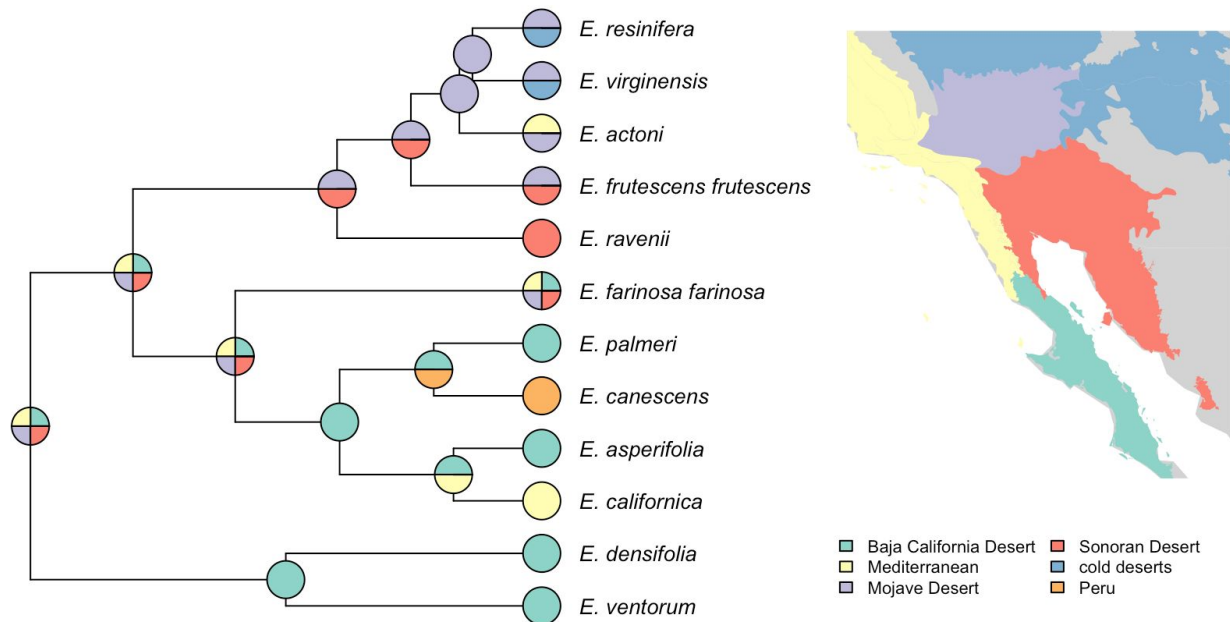
Figure S1: Ancestral range reconstruction in *Encelia* based on the DEC model implemented in `BioGeoBEARS`. Left shows phylogeny; pie charts at tips show the biogeographic ranges to which species were assigned and pie charts at nodes represent the ancestral range reconstruction with the highest probability at that node. The map shows the biogeographic regions.
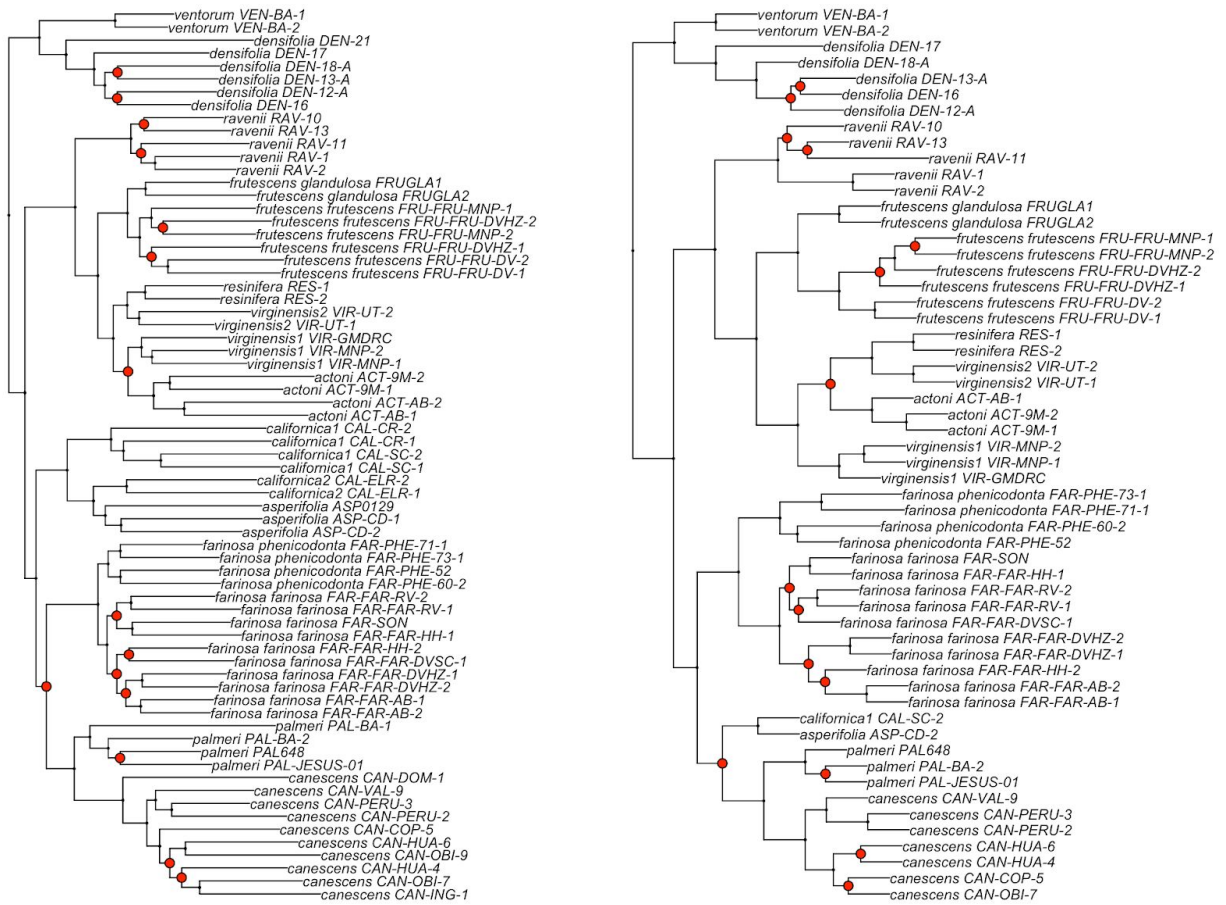
Figure S2: Individual-level phylogenies for *Encelia* inferred using (L) a concatenated maximum-likelihood approach implemented in RAxML and (R) a single nucleotide polymorphism (SNP) coalescent-based approach implemented in SVDquartets. The SVDquartets phylogeny (n = 56) contains a subset of the tips in the RAxML phylogeny (n = 69) because individuals with high levels of missing SNP data were removed. Phylogenies rooted by outgroups (not shown). Nodes labeled in red differ between the two topologies. Most of the nodes that differ are among individuals within a species.
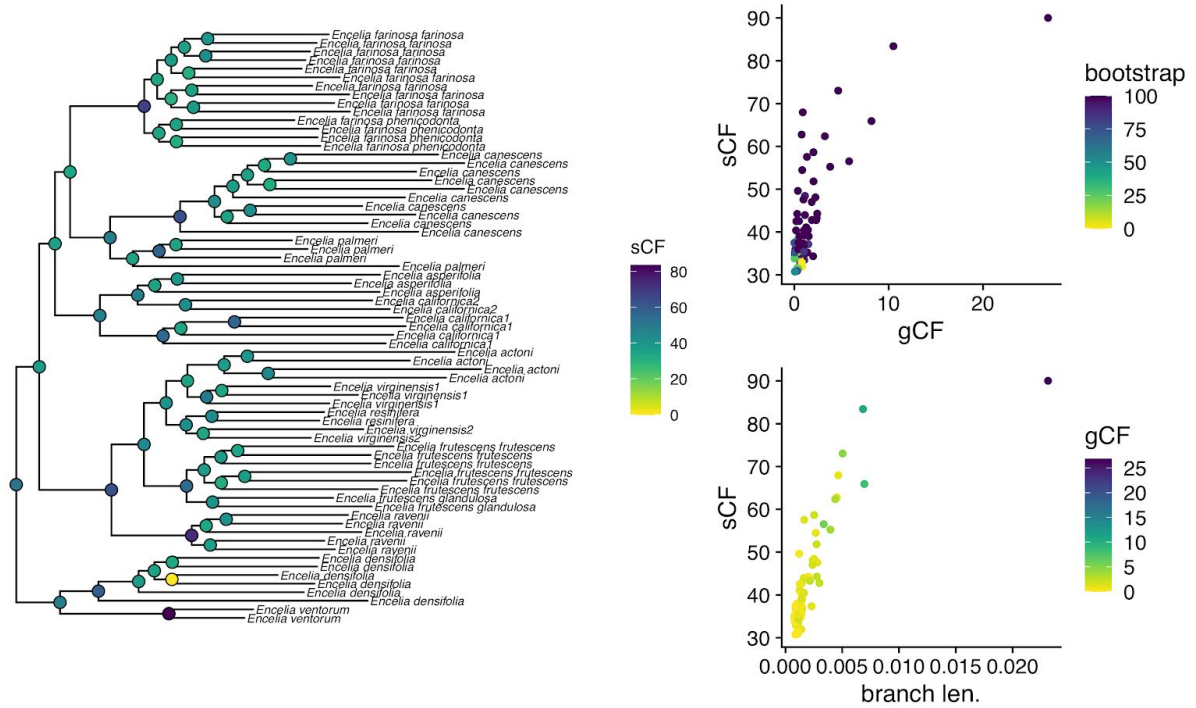
Figure S3: Individual-level phylogenies for *Encelia* inferred using a concatenated maximum-likelihood approach implemented in RAxML. Phylogeny rooted by outgroups (not shown). Nodal values indicate site concordance factors (sCF). Plots show (top) gene concordance factors (gCF) relative to sCF and (bottom) sCF relative to branch length. sCF and gCF values are relatively low throughout the topology. Low sCF and gCF values are expected in recent rapid radiations due to extensive incomplete lineage sorting.
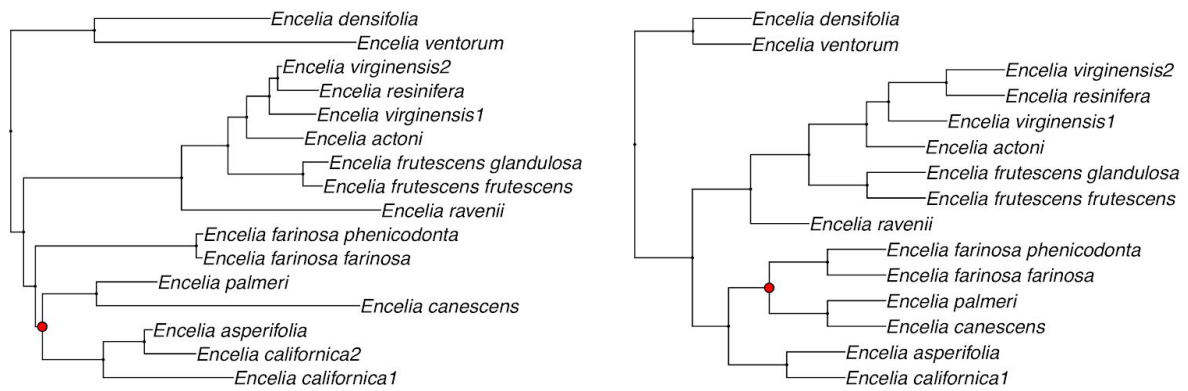
Figure S4: Lineage-level phylogenies inferred using coalescent-based approaches (L) using gene trees implemented in ASTRAL and (R) single nucleotide polymorphisms implemented in SVDquartets. Nodes that differ between the two topologies shown in red. The sole node that differs between the two topologies has low local posterior probability (0.93; Fig. 2).
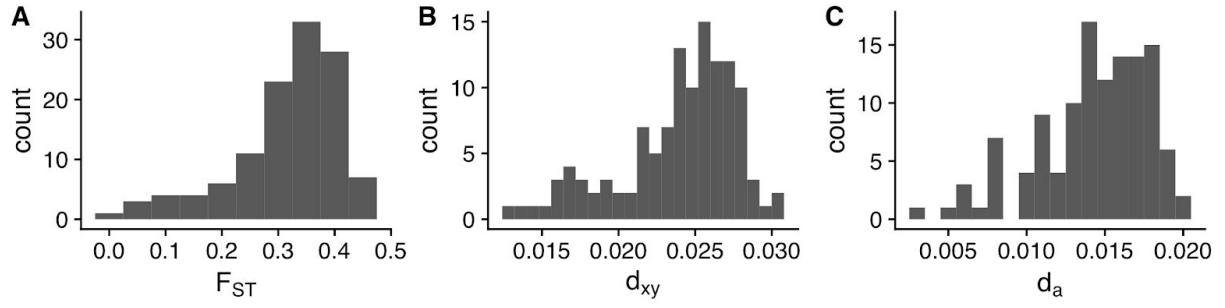
Figure S5: Genetic divergence between *Encelia* species, as measured by (A) F_{ST}, (B) d_{xy}, and (C) d_a. As expected under a recent, rapid radiation, genetic divergences across species-pairs are both low and similar.
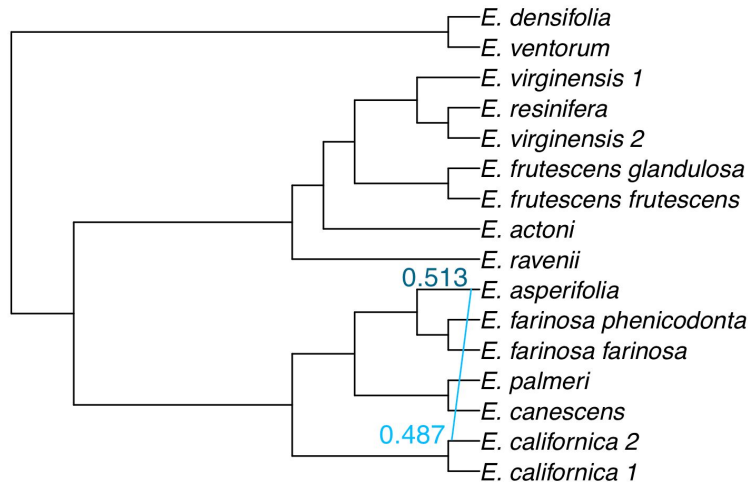
Figure S6: Reconstruction of *Encelia*'s evolutionary history as a network using SNaQ. The best fit model inferred one reticulation event; *E. asperifolia* is a hybrid with ~50% ancestry of *E. californica 2*. *Encelia asperifolia* has been hypothesized to be a hybrid species resulting from hybridization between *E. californica* and *E. frutescens glandulosa* (Table S4), although this hypothesis has not been formally tested previously.
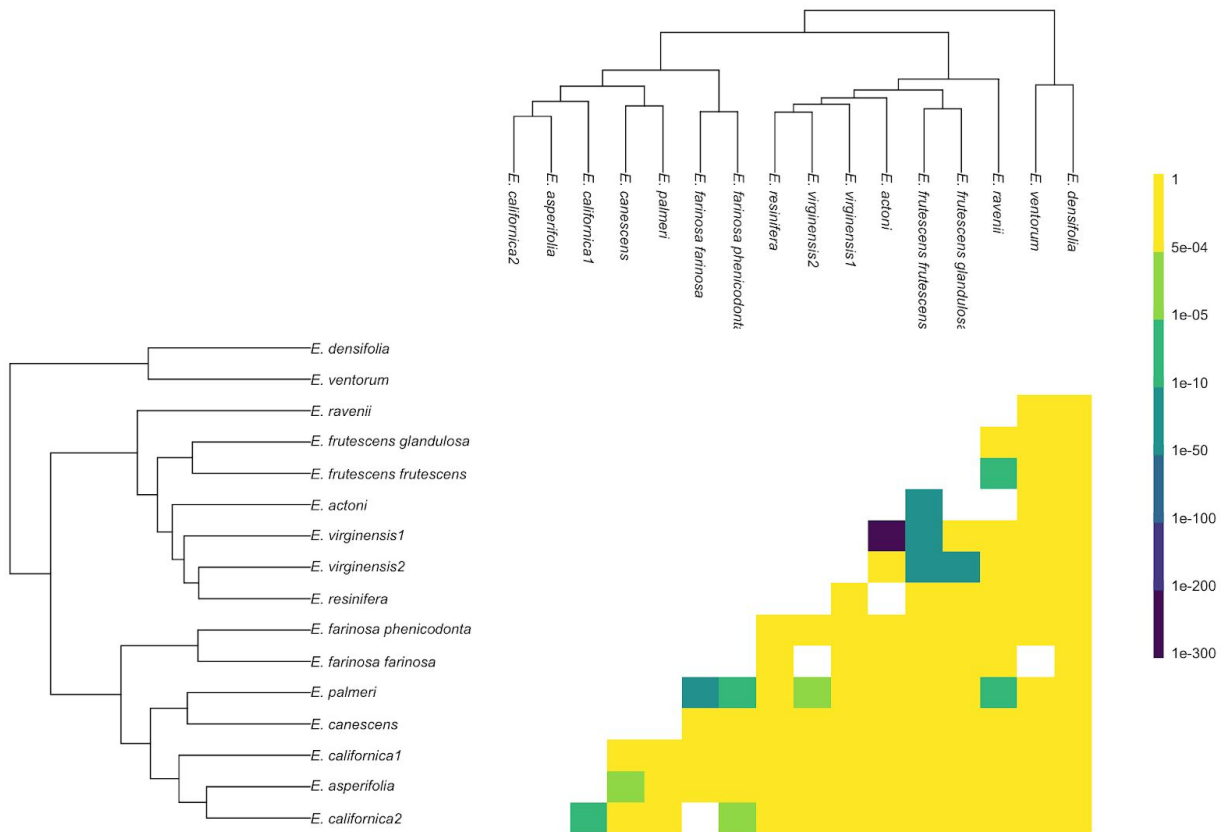
Figure S7: Introgression across *Encelia* as measured by the D-statistic. Plotted are the p-values of measured D-statistics (Table S3). The D-statistic was calculated across all possible triads in *Encelia*; for a given species pair, shown is the greatest p-value. Insignificant tests are shown in yellow; all significant tests are shown in shades of green & blue. Some species pairs are shown in white. For these species pairs, we either could not evaluate the D-statistic because they are sister species or because, in all comparisons involving these two species, introgression occurred with the third species. Even using this conservative approach, several species-pairs show strong evidence for introgression, including some species known to hybridize in nature (Fig. 3).
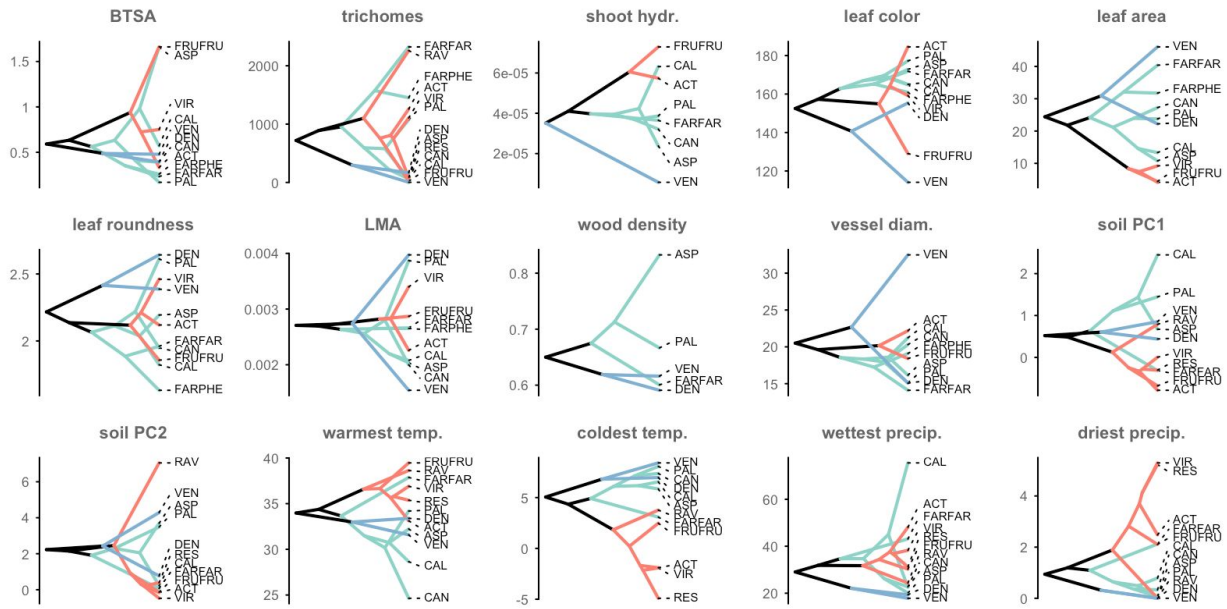
Figure S8: Phenotypic variation in *Encelia*, depicted as phenograms. The y-axis indicates phenotypic spread across (top two rows) morphological and physiological traits and (bottom row) environmental variation. Trait abbreviations follow Table 1. Branches are colored by clade identity as shown in Fig. 2, and all species names are abbreviated to the first three characters. Closely-related species in *Encelia* often exhibit dramatically different phenotypes.
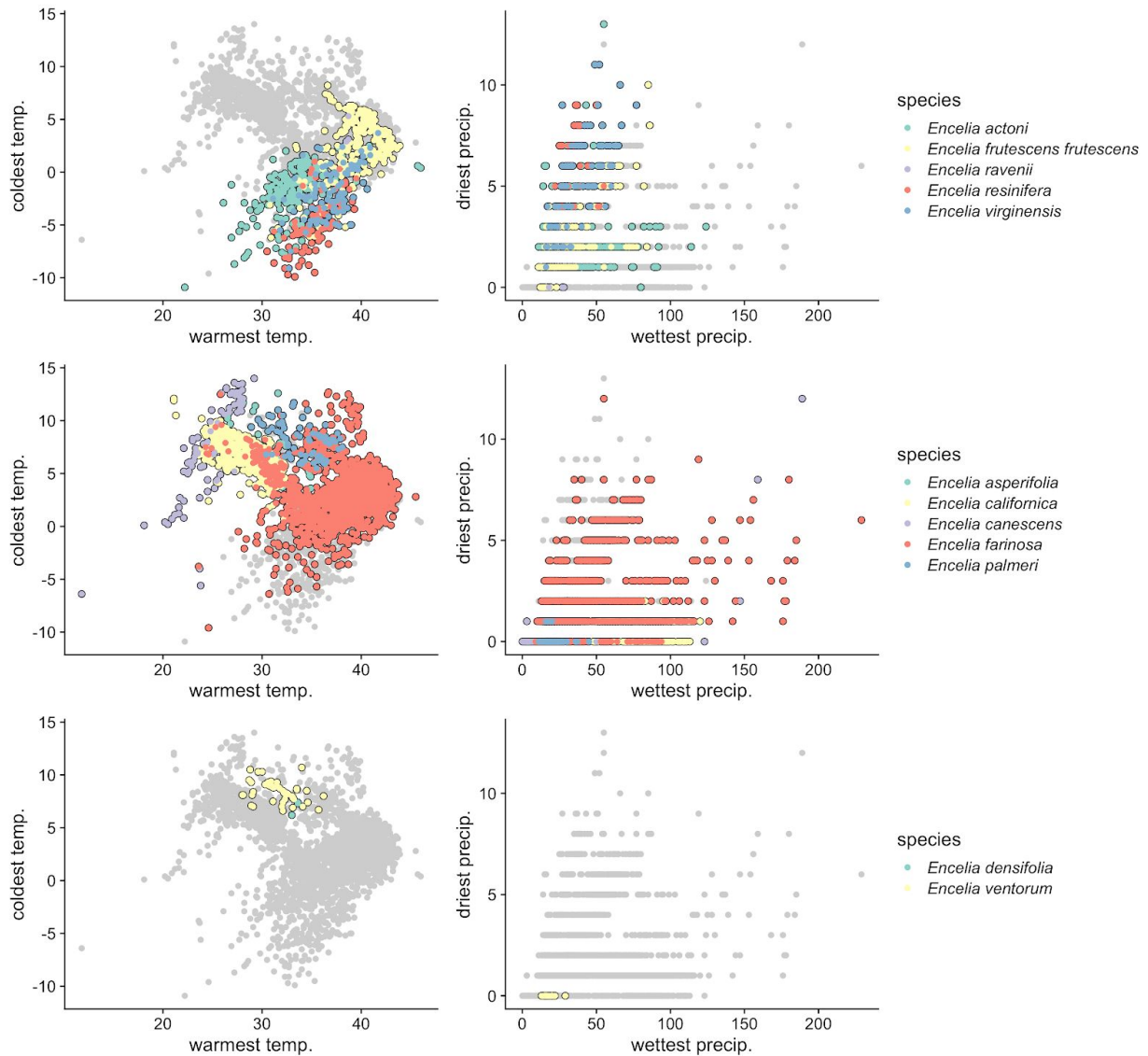
Figure S9: The environmental space occupied by *Encelia* species, as summarized by four bioclimatic variables: maximum temperature of the warmest month (BIO5), minimum temperature of the coldest month (BIO6), precipitation of wettest month (BIO13), and precipitation of driest month (BIO14). Species are broken up by the major clades in which they occur (Fig. 2). The species in *Encelia* occupy a diversity of climatic environments, although many of them overlap in climatic space.
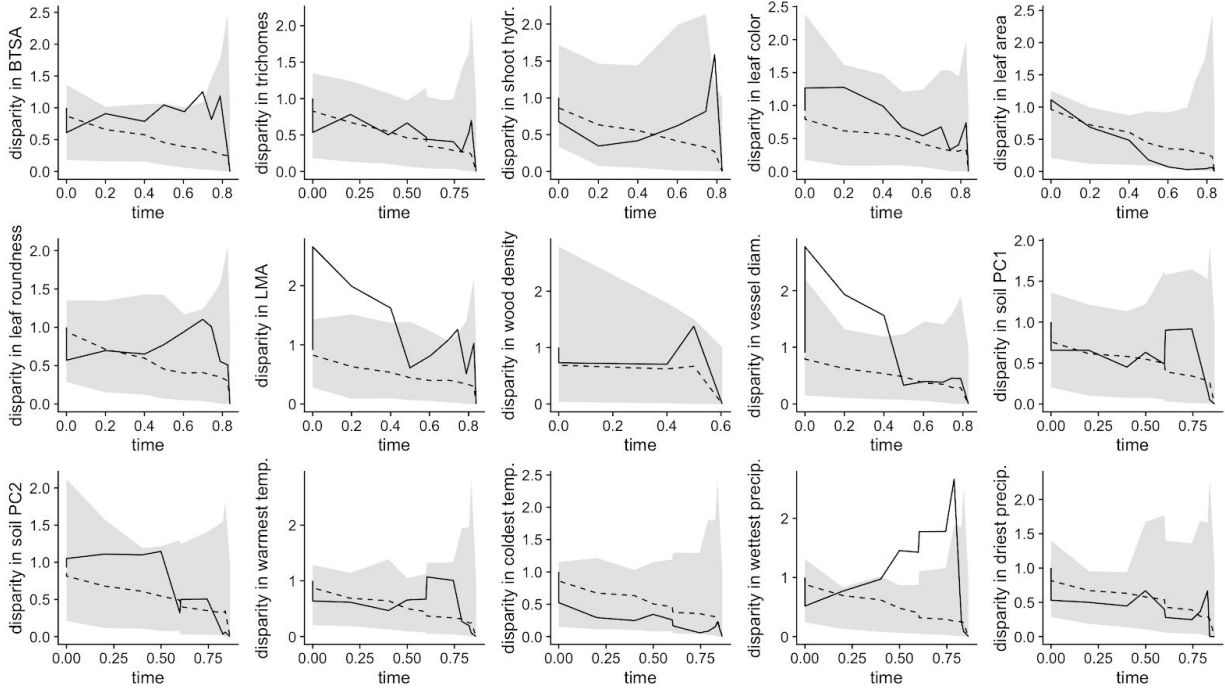
Figure S10: Disparity-through-time plots for phenotypic variation in morphological traits and environmental space. Solid black lines show disparity as measured in *Encelia*. The gray area indicates the 95% confidence interval across 100 simulations and the dotted black lines indicate the mean across Brownian motion simulations. Unlike many adaptive radiations, *Encelia* does not show evidence of early disparification.
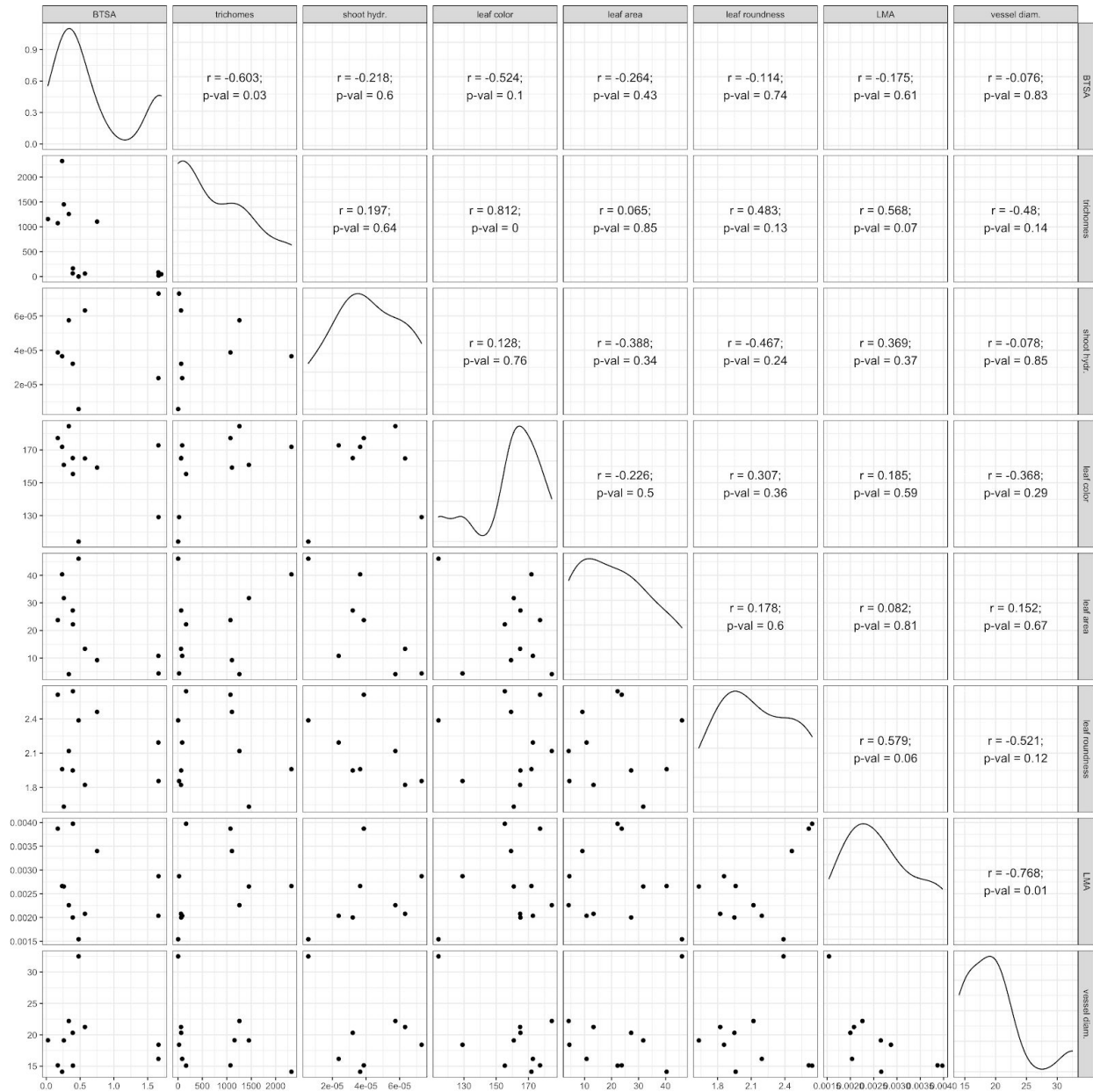
Figure S11: Pairwise correlations among all measured traits in *Encelia* (Table S2). Wood density was excluded due to low sample size. Shown in the upper diagonal are estimates of phylogenetic correlations and p-values between ln-transformed traits. Very few traits are correlated strongly |r > 0.6| and even fewer are significantly correlated. One of the few significant correlations is between leaf color and trichome density; this is expected as a high density of trichomes can result in a leaf looking more white.
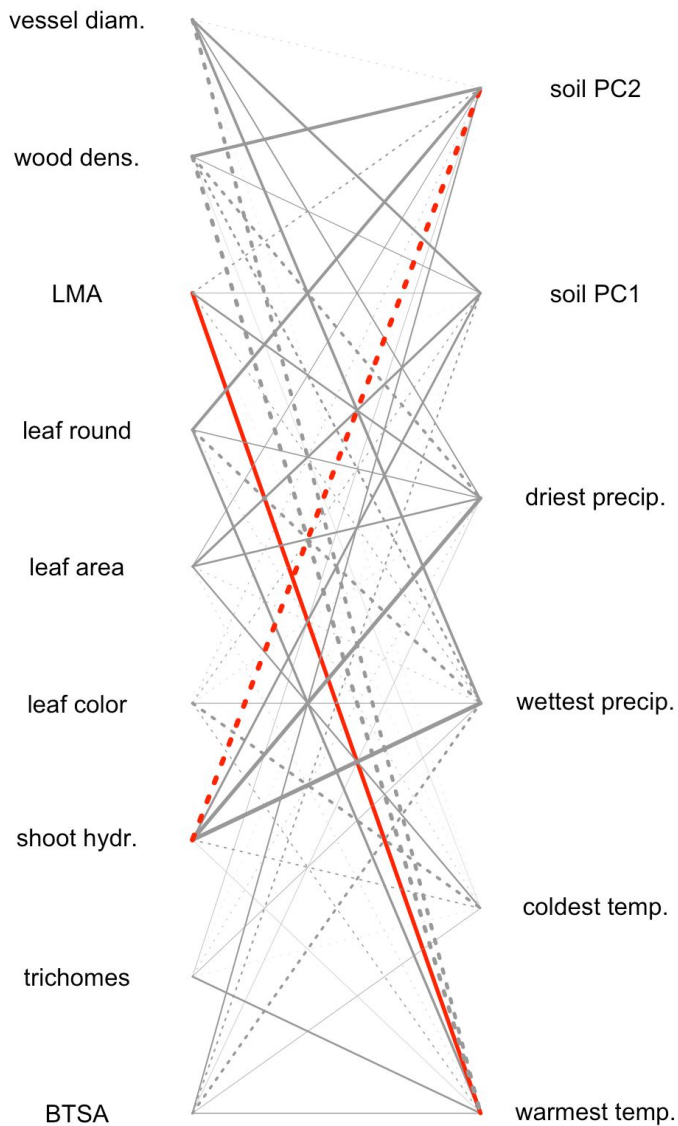
Figure S12: Correlations between (L) trait and (R) environmental variables. Trait abbreviations follow Table 1. Width of lines indicate absolute strength of phylogenetic correlation between ln-transformed traits and environment. Red lines indicate significant correlations ($p < 0.05$), and dotted lines indicate negative correlations. Very few traits are correlated significantly with environmental variation.